Available online at www.sciencedirect.com
ScienceDirect
Journal of Computational Physics 221 (2007) 269–287
JOURNAL OF COMPUTATIONAL PHYSICS
www.elsevier.com/locate/jcp

Computing unstable periodic waves at the interface of two inviscid fluids in uniform vertical flow

Lawrence K. Forbes *, Michael J. Chen, Claire E. Trenham

School of Mathematics and Physics, University of Tasmania, Private Bag 37, Hobart 7001, Tasmania, Australia

Received 11 December 2005; received in revised form 5 June 2006; accepted 9 June 2006
Available online 28 July 2006

Abstract

Periodic waves at the interface of two immiscible fluids are considered. Each fluid is inviscid and incompressible, and is moving vertically with constant speed. The upper fluid is more dense than the lower one, and the interface between them is thus unstable to small perturbations. A linearized solution, valid for waves of small amplitude, is reviewed and a novel numerical method is presented for computing waves of moderate amplitude. The technique uses a Fourier–Galerkin approach, and converts the governing equations into a system of ordinary differential equations for the Fourier coefficients. It is then shown how the method may be modified to allow for the evolution of overhanging waves, using a novel time-dependent arclength formulation.

Keywords: Fluid interface; Incompressible flow; Irrotational flow; Periodic waves; Spectral methods; Unstable flow

1. Introduction

The study of an unstable interface between two fluids has a long history, beginning with the work of Helmholtz, Kelvin and Rayleigh. When the two fluid layers move parallel to the horizontal interface, waves at that boundary may be unstable, depending on the speeds in the two fluid layers. This is the famous Kelvin–Helmholtz instability, and is discussed in article 232 of Lamb [1], and in Chandrasekhar ([2], chapter 11). Alternatively, a heavier fluid may overlie a lighter one, so that the motion of the fluid system is orthogonal to the interface. When the vertical motion occurs with constant acceleration, the resulting unstable flow is known as the Rayleigh–Taylor instability. The original article on the topic is that by Rayleigh [3] and the flow was analyzed later in a famous paper by Taylor [4].

Rayleigh–Taylor instability has subsequently been the subject of extensive investigation. The literature on the topic is too great to survey here, and we refer instead to the major review articles by Sharp [5], Kull [6] and Inogamov [7]. As the instability evolves at the interface, descending spikes of the heavier fluid can penetrate

* Corresponding author.
E-mail address: larry.forbes@utas.edu.au (L.K. Forbes).

0021-9991/$ - see front matter
doi:10.1016/j.jcp.2006.06.010

into the lighter lower one, and a similarity solution of the development of the tip has been presented recently by Clavin and Williams [8].

The Rayleigh–Taylor instability is now believed to occur in a variety of physical circumstances, arising in geology, oceanography, industry and astrophysics. Some technological situations involving the Rayleigh–Taylor instability in industrial applications are discussed by Sharp [5], for example. In astrophysics, the birth of a star can be associated with the presence of a region of lower density gas that expands into a heavier inter-stellar medium. Eventually, the expanding interface at the edge of this gaseous region is believed to become Rayleigh–Taylor unstable, and to lose its initial spherical shape, so developing large-amplitude perturbations known as "super-bubbles", "chimneys" and "worms". This effect has been modelled numerically by de Avillez and Berry [9], who used an adaptive, shock-capturing finite-difference method to solve the equations of motion for a compressible inviscid gas with energy input from supernova events and an energy loss term due to radiation. A detailed observational study of the small-scale structure of a particular "chimney" has been presented by McClure-Griffiths et al. [10] using the Australia telescope compact array and Parkes facilities, and appears to confirm the importance of the Rayleigh–Taylor instability as a mechanism for the generation of "chimneys".

The present paper focusses on a flow related to the Rayleigh–Taylor instability, but in which the fluids move vertically with constant speed rather than constant acceleration. Such a problem is also believed to be of importance in the astrophysical context, and is associated with the Richtmyer–Meshkov instability (see, for example Brouillette [11]), in which a shock wave is responsible for impulsive acceleration of an interface. At longer times, this may give rise to constant-velocity growth of initial perturbations on the interface, as has been discussed by Kull [6]. A similar phenomenon may occur in reservoirs or in the ocean as a result of the upwelling of lighter fluid from some region deep within the fluid system, and the consequent appearance of descending plumes of heavier fluid. This type of situation is discussed in the oceanographic context by Lazier et al. [12].

The governing equations are presented in Section 2, and the linearized solution is reviewed briefly in Section 3. The essential numerical scheme is outlined in Section 4, and is based on the use of straightforward Fourier series. However, it employs a novel technique of differentiating one of the kinematic free surface conditions with respect to time, so that a system of ordinary differential equations may be derived for the coefficients in the Fourier series. These may then be integrated in a straightforward fashion, to reveal the time-dependent behaviour of the interface. To some extent, this method is an extension and generalization of the Fourier techniques used by Fenton and Rienecker [13] and Dommermuth and Yue [14] for computing periodic water waves, and by Kim et al. [15] for more general inviscid flows in tanks of finite width. It is an additional feature of the present work that the interfacial profiles may fold into mushroom-shaped configurations as time increases, so that overhanging portions may be present. This requires a modification of the numerical scheme, to allow multiple-valued interface elevations to be computed. We do this here using a time-dependent arc-length method, which is described in Section 5. Results of computation are discussed in Section 6, and the paper concludes with a discussion in Section 7.

2. The governing equations

Consider two fluids separated by a horizontal interface, and locate a cartesian coordinate system with the x-axis running horizontally along the interface, and the y-axis pointing vertically. The fluids are subject to the gravitational body force, directed downwards (in the negative y-direction) with acceleration g. Upper fluid 2 has density ρ_2 and the lower fluid 1 has density ρ_1, following the notation in Batchelor ([16], p. 69). We assume in this paper that $\rho_2 > \rho_1$, so that the upper fluid is more dense than the lower one, and the entire two-fluid system is consequently unstable. The fluids are being driven with constant speed V from below, and in the absence of perturbations, the interface would remain horizontal with location given simply by the equation $y = Vt$, in which t denotes time. However, it is assumed that the interface does not remain undisturbed, but is subject to a periodic perturbation, with wavelength λ in the x-direction.

Non-dimensional variables are now introduced, and will be used throughout the rest of this paper. All lengths are scaled relative to the inverse wavenumber $\lambda/2\pi$ and speeds are referenced to the upwelling speed

V. Time is made non-dimensional by referring it to the characteristic time $\lambda/(2\pi V)$. It is found that the problem thus depends on the two dimensionless parameters F and D, defined by the relations

$$F^2 = \frac{2\pi V^2}{g\lambda}, \quad D = \frac{\rho_2}{\rho_1}. \tag{2.1}$$

The constant F is effectively a Froude number based on the upwelling speed V and wavelength λ, and D is the density ratio; in this paper, it is assumed that $D > 1$.

Each fluid is assumed to be incompressible and to flow irrotationally, so that velocity potentials ϕ_1 and ϕ_2 exist in the two fluid layers. In each fluid, the velocity has components u and v in the x- and y-directions, respectively, and thus

$$(u_i, v_i) = \left(\frac{\partial \phi_i}{\partial x}, \frac{\partial \phi_i}{\partial y}\right) \quad \text{for } i = 1, 2. \tag{2.2}$$

It follows that Laplace's equation

$$\nabla^2 \phi_i = 0 \quad \text{for } i = 1, 2 \tag{2.3}$$

is satisfied in each fluid layer; in addition, the fluids far from the interface must be moving vertically with unit non-dimensional speed, so that:

$$\begin{aligned} u_1 &\to 0, \quad v_1 \to 1 \quad \text{as } y \to -\infty \\ u_2 &\to 0, \quad v_2 \to 1 \quad \text{as } y \to \infty. \end{aligned} \tag{2.4}$$

Let the location and shape of the interface be described by the equation $y = \eta(x, t)$. Each fluid must satisfy a kinematic condition

$$v_i = \frac{\partial \eta}{\partial t} + u_i \frac{\partial \eta}{\partial x} \quad \text{for } i = 1, 2 \quad \text{on } y = \eta \tag{2.5}$$

representing the fact that neither fluid is permitted to cross the interface. There is also a dynamic condition that the pressures either side of the interface must be equal. In each fluid, the pressure is able to be computed by means of Bernoulli's equation (see Batchelor [16], p. 387) and equating the two gives

$$D\frac{\partial \phi_2}{\partial t} - \frac{\partial \phi_1}{\partial t} + \frac{1}{2}D(u_2^2 + v_2^2) - \frac{1}{2}(u_1^2 + v_1^2) + \frac{(D-1)}{F^2}\eta = \frac{1}{2}(D-1) + \frac{(D-1)}{F^2}t \quad \text{on } y = \eta. \tag{2.6}$$

A sketch of the dimensionless problem is given in Fig. 1.

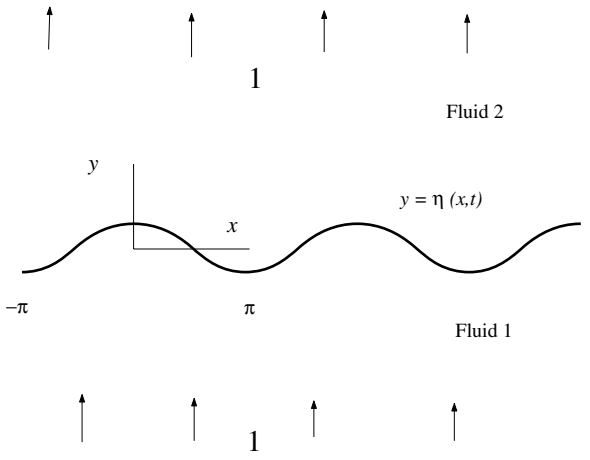

Fig. 1. Definition sketch of the two-fluid system and the periodic interface (which is taken from an actual solution). Flow occurs vertically, with dimensionless speed 1 far from the interface.

It is convenient now to transform Eqs. (2.2)–(2.6) into a new cartesian coordinate system (x, Y) that moves with the interface. Accordingly, we write:

$$\begin{aligned} y &= t + Y, \\ \eta(x,t) &= t + H(x,t) \end{aligned} \tag{2.7}$$

and transform the governing equations into this new coordinate system, using the chain rule of calculus. Once this has been done, it is then appropriate to introduce perturbed velocity potentials Φ_1 and Φ_2 in each fluid layer, by means of the expressions

$$\phi_i = Y + t + \Phi_i \quad \text{for } i = 1, 2. \tag{2.8}$$

It may be shown that Laplace's equations (2.3) take the forms:

$$\begin{aligned} \frac{\partial^2 \Phi_1}{\partial x^2} + \frac{\partial^2 \Phi_1}{\partial Y^2} &= 0 \quad \text{in } Y < H(x,t), \\ \frac{\partial^2 \Phi_2}{\partial x^2} + \frac{\partial^2 \Phi_2}{\partial Y^2} &= 0 \quad \text{in } Y > H(x,t), \end{aligned} \tag{2.9}$$

and the limiting conditions (2.4) become simply:

$$\begin{aligned} \nabla \Phi_1 &\to 0 \quad \text{as } Y \to -\infty, \\ \nabla \Phi_2 &\to 0 \quad \text{as } Y \to \infty \end{aligned} \tag{2.10}$$

in terms of the new variables defined in Eqs. (2.7) and (2.8). The kinematic conditions (2.5) become

$$\frac{\partial \Phi_i}{\partial Y} = \frac{\partial H}{\partial t} + \frac{\partial \Phi_i}{\partial x}\frac{\partial H}{\partial x} \quad \text{for } i = 1, 2 \quad \text{on } Y = H(x,t) \tag{2.11}$$

and the final form of the dynamic condition (2.6) is

$$D\frac{\partial \Phi_2}{\partial t} - \frac{\partial \Phi_1}{\partial t} + \frac{1}{2}D\left[\left(\frac{\partial \Phi_2}{\partial x}\right)^2 + \left(\frac{\partial \Phi_2}{\partial Y}\right)^2\right] - \frac{1}{2}\left[\left(\frac{\partial \Phi_1}{\partial x}\right)^2 + \left(\frac{\partial \Phi_1}{\partial Y}\right)^2\right] + \frac{(D-1)}{F^2}H = 0 \quad \text{on } Y = H(x,t). \tag{2.12}$$

We seek unsteady solutions to this governing system of equations (2.9)–(2.12), in the unstable situation $D > 1$. In these dimensionless coordinates, the waves have periodicity 2π along the x-axis, and without loss of generality we choose the crest of a wave to lie on the y-axis, as illustrated in Fig. 1. Thus the wave profile may be assumed to be symmetric about the moving Y-axis in the analysis to follow.

3. The linearized solution

This section briefly reviews the solution to a linearized approximation of the governing equations (2.9)–(2.12), assuming that both fluids are initially at rest and that the interface initially has a simple cosine profile. The analysis is only valid for small values of a wave amplitude ϵ, and makes use of perturbation expressions for the velocity potentials and surface heights, in the form:

$$\begin{aligned} \Phi_1(x,Y,t) &= \epsilon A_1(t) \mathrm{e}^{Y} \cos x + \mathcal{O}(\epsilon^2), \\ \Phi_2(x,Y,t) &= \epsilon A_2(t) \mathrm{e}^{-Y} \cos x + \mathcal{O}(\epsilon^2), \\ H(x,t) &= \epsilon H_1(t) \cos x + \mathcal{O}(\epsilon^2). \end{aligned} \tag{3.1}$$

The first two quantities in the system (3.1) are the perturbed velocity potentials, and have been chosen so that they satisfy Laplace's equation in each region and the appropriate limiting conditions far away from the interface, according to Eqs. (2.9) and (2.10).

At time $t = 0$ both fluids are at rest and there is a sinusoidal disturbance to the interface, and so the appropriate initial conditions are

$$A_1(0) = 0, \quad A_2(0) = 0, \quad H_1(0) = 1. \tag{3.2}$$

It is possible to consider different starting conditions to these, although this is the only situation discussed in this section. It will be seen later, however, that the choice of initial conditions is a key factor in determining the large amplitude behaviour that develops as time increases.

The kinematic and dynamic conditions at the interface are linearized in the usual way, making use of Taylor series expansions to project variables evaluated at the true interface $Y = H$ onto the approximate surface $Y = 0$ and disregarding terms of order ϵ^2 and higher. The two kinematic conditions (2.11) become approximately

$$A_1(t) = -A_2(t) = \frac{\mathrm{d}H_1(t)}{\mathrm{d}t} \tag{3.3}$$

and the dynamic condition (2.12) reduces to

$$\frac{\mathrm{d}^2 H_1}{\mathrm{d}t^2} - \frac{(D-1)}{F^2(D+1)} H_1 = 0, \tag{3.4}$$

after use has been made of (3.1) and (3.3).

It is now straightforward to solve the linearized system (3.1)–(3.4), and the calculations are similar to those presented in the famous paper of Taylor [4]. The final form of the solution is found to be:

$$\begin{aligned} \Phi_1(x, Y, t) &= \epsilon r \sinh(rt) \mathrm{e}^{Y} \cos x + \mathcal{O}(\epsilon^2), \\ \Phi_2(x, Y, t) &= -\epsilon r \sinh(rt) \mathrm{e}^{-Y} \cos x + \mathcal{O}(\epsilon^2), \\ H(x, t) &= \epsilon \cosh(rt) \cos x + \mathcal{O}(\epsilon^2), \end{aligned} \tag{3.5}$$

in which it is convenient to define the parameter

$$r = \sqrt{\frac{(D-1)}{F^2(D+1)}}, \tag{3.6}$$

in the unstable case for which the density ratio $D > 1$. The quantity r^2F^2 is sometimes referred to as the Atwood number (see [11], for example).

It follows from the solution (3.5) that the instability develops only slowly as density ratio $D \to 1$, since the parameter in Eq. (3.6) behaves as $r \to 0$ in that limit. Conversely, the slower the upwelling speed, the more rapidly the instability develops, since $r \to \infty$ as $F \to 0$. However, for a non-zero Froude number F, there is a limit to how rapidly the unstable interface can evolve, since then r in Eq. (3.6) is bounded above by the quantity $1/F$, even as the density ratio becomes infinite, $D \to \infty$.

4. The basic numerical solution

We seek a solution of period 2π to the governing equations (2.9)–(2.12). In order to satisfy Laplace's equation (2.9) and the limiting conditions (2.10) it is therefore necessary to take

$$\Phi_1(x, Y, t) = P_0(t) + \sum_{n=1}^{N} P_n(t) \mathrm{e}^{nY} \cos(nx) \tag{4.1}$$

and

$$\Phi_2(x, Y, t) = Q_0(t) + \sum_{n=1}^{N} Q_n(t) \mathrm{e}^{-nY} \cos(nx). \tag{4.2}$$

The perturbed interface is likewise an even periodic function of x, and so it takes the form

$$H(x, t) = H_0(t) + \sum_{n=1}^{N} H_n(t) \cos(nx). \tag{4.3}$$

The number N of Fourier coefficients in the expressions (4.1)–(4.3) may be taken to be arbitrarily large. In fact, the two coefficients P_0 and Q_0 are not actually needed in the final numerical solution, since it is only the spatial derivatives of the velocity potentials in (4.1) and (4.2) that have physical meaning. We set $P_0(t) = 0$, but solve for $Q_0(t)$ in the scheme to follow.

It remains to satisfy the two kinematic conditions (2.11) and the dynamic condition (2.12) on the interface $Y = H$. Expressions (4.1) and (4.3) are substituted into the first kinematic condition for lower fluid 1 in the system (2.11), to yield a form of the equation that involves the Fourier coefficients. This new equation is then Fourier decomposed, by multiplying successively by the basis functions $\cos(jx)$, $j = 0, 1, \ldots, N$ and integrating over the interval $[-\pi, \pi]$. This results in

$$2\pi H_0'(t) = \sum_{n=1}^{N} P_n(t) \int_{-\pi}^{\pi} n\mathrm{e}^{nH} \cos(nx)\,\mathrm{d}x - \int_{-\pi}^{\pi} \left(\frac{\partial \Phi_1}{\partial x}\right)_{Y=H} \frac{\partial H}{\partial x}\,\mathrm{d}x \tag{4.4}$$

and

$$\pi H_j'(t) = \sum_{n=1}^{N} P_n(t) \int_{-\pi}^{\pi} n\mathrm{e}^{nH} \cos(nx)\cos(jx)\,\mathrm{d}x - \int_{-\pi}^{\pi} \left(\frac{\partial \Phi_1}{\partial x}\right)_{Y=H} \frac{\partial H}{\partial x}\cos(jx)\,\mathrm{d}x \quad \text{for } j = 1, \ldots, N. \tag{4.5}$$

When the series expression (4.1) is substituted into the second integral on the right-hand side of Eq. (4.4), that term is then able to be transformed using integration by parts. Remarkably, both terms on the right-hand side of (4.4) cancel exactly, leaving simply

$$H_0'(t) = 0. \tag{4.6}$$

This leads at once to the following result:

Theorem. *The mean perturbed interface height is invariant with time.*

Proof. The rate of change of the average value of the perturbed interface height is

$$\frac{\mathrm{d}}{\mathrm{d}t}\left[\frac{1}{2\pi}\int_{-\pi}^{\pi} (\eta(x,t) - t)\,\mathrm{d}x\right].$$

By Eqs. (2.7) and (4.3), this expression may be calculated to have the value $H_0'(t)$, which is zero from Eq. (4.6). Thus the mean value of the perturbed interface height is independent of time, as required. □

It follows in particular from this theorem that, if the initial mean value of the perturbed interface height is zero, then it must remain so for all subsequent times. In that case, the average value of the elevation η is simply the undisturbed value $y = t$.

Eq. (4.5) may similarly be integrated by parts, after use is made of the series expression (4.1). This yields the simpler result

$$\pi H_j'(t) = j\sum_{n=1}^{N} P_n(t) \int_{-\pi}^{\pi} \mathrm{e}^{nH} \sin(nx)\sin(jx)\,\mathrm{d}x \quad \text{for } j = 1, \ldots, N. \tag{4.7}$$

The second of the kinematic conditions in the system (2.11), for upper fluid 2, may be treated in a similar way to the above, first multiplying by basis functions $\cos(jx)$ and then integrating by parts. The zeroth mode $j = 0$ again gives rise to the result in Eq. (4.6), and the remaining modes give

$$\pi H_j'(t) = -j\sum_{n=1}^{N} Q_n(t) \int_{-\pi}^{\pi} \mathrm{e}^{-nH} \sin(nx)\sin(jx)\,\mathrm{d}x \quad \text{for } j = 1, \ldots, N. \tag{4.8}$$

The right-hand side of Eqs. (4.7) and (4.8) are equated, and the resulting expression is then differentiated with respect to time. This yields a system in the form

$$\sum_{n=1}^{N} (S_{jn}^{(1)} P_n'(t) + S_{jn}^{(2)} Q_n'(t)) = \sum_{n=1}^{N} n(K_{jn}^{(2)} Q_n(t) - K_{jn}^{(1)} P_n(t)) \quad \text{for } j = 1, \ldots, N, \tag{4.9}$$

in which it is convenient to define the intermediate quantities:

$$\begin{aligned}
S_{jn}^{(1)}(t) &= \int_{-\pi}^{\pi} \mathrm{e}^{nH} \sin(nx)\sin(jx)\,\mathrm{d}x,\\
S_{jn}^{(2)}(t) &= \int_{-\pi}^{\pi} \mathrm{e}^{-nH} \sin(nx)\sin(jx)\,\mathrm{d}x,\\
K_{jn}^{(1)}(t) &= \int_{-\pi}^{\pi} \mathrm{e}^{nH}\left[\frac{\partial \Phi_1}{\partial Y} - \frac{\partial \Phi_1}{\partial x}\frac{\partial H}{\partial x}\right]_{Y=H} \sin(nx)\sin(jx)\,\mathrm{d}x,\\
K_{jn}^{(2)}(t) &= \int_{-\pi}^{\pi} \mathrm{e}^{-nH}\left[\frac{\partial \Phi_2}{\partial Y} - \frac{\partial \Phi_2}{\partial x}\frac{\partial H}{\partial x}\right]_{Y=H} \sin(nx)\sin(jx)\,\mathrm{d}x
\end{aligned} \tag{4.10}$$

after use has been made of the kinematic conditions (2.11).

Finally, the dynamic surface condition (2.12) is also treated by Fourier decomposition, multiplying by the basis functions $\cos(jx)$, $j = 0, 1, \ldots, N$ and integrating as before. For the mean component with $j = 0$, the Fourier decomposition of the dynamic condition gives rise to the equation

$$2\pi D Q_0'(t) + D\sum_{n=1}^{N} C_{0n}^{(2)} Q_n'(t) - \sum_{n=1}^{N} C_{0n}^{(1)} P_n'(t) = -\frac{1}{2} D J_0^{(2)} + \frac{1}{2} J_0^{(1)} - \frac{2\pi(D-1)}{F^2} H_0(t). \tag{4.11}$$

In addition, the higher-mode terms in the Fourier analysis of (2.12) yield

$$D\sum_{n=1}^{N} C_{jn}^{(2)} Q_n'(t) - \sum_{n=1}^{N} C_{jn}^{(1)} P_n'(t) = -\frac{1}{2} D J_j^{(2)} + \frac{1}{2} J_j^{(1)} - \frac{\pi(D-1)}{F^2} H_j(t) \quad \text{for } j = 1, \ldots, N. \tag{4.12}$$

In Eqs. (4.11) and (4.12), it has again proved convenient to define intermediate quantities:

$$\begin{aligned}
C_{jn}^{(1)}(t) &= \int_{-\pi}^{\pi} \mathrm{e}^{nH} \cos(nx)\cos(jx)\,\mathrm{d}x,\\
C_{jn}^{(2)}(t) &= \int_{-\pi}^{\pi} \mathrm{e}^{-nH} \cos(nx)\cos(jx)\,\mathrm{d}x,\\
J_{j}^{(1)}(t) &= \int_{-\pi}^{\pi} \left[\left(\frac{\partial \Phi_1}{\partial x}\right)^2 + \left(\frac{\partial \Phi_1}{\partial Y}\right)^2\right]_{Y=H} \cos(jx)\,\mathrm{d}x,\\
J_{j}^{(2)}(t) &= \int_{-\pi}^{\pi} \left[\left(\frac{\partial \Phi_2}{\partial x}\right)^2 + \left(\frac{\partial \Phi_2}{\partial Y}\right)^2\right]_{Y=H} \cos(jx)\,\mathrm{d}x.
\end{aligned} \tag{4.13}$$

Eqs. (4.7), (4.9), (4.11) and (4.12) constitute a matrix system of $3N + 1$ ordinary differential equations, to be solved for the $3N + 1$ unknown functions $H_n(t)$, $P_n(t)$, $Q_n(t)$, $n = 1, 2, \ldots, N$ and $Q_0(t)$, after it has been assumed that $P_0(t) = 0$ and $H_0(t) = 0$ using the theorem above. This system may be solved using any convenient numerical integration routine, and we used the standard fourth-order Runge–Kutta method in Atkinson ([17], p. 371). The integrals in the intermediate quantities (4.10) and (4.13) have been evaluated using the trapezoidal rule, which is exponentially accurate for these periodic integrands (see Atkinson ([17], p. 253)), and exploiting the fact that the integrands are even functions in each of these expressions.

This method works well and is capable of computing the evolution of unstable periodic waves in this system. It is found in many instances, however, that the interface may develop vertical portions in its profile, and so the technique described so far necessarily fails when this occurs. It may be extended, however, to allow the calculation of steeper and even overturning unstable waves, and this technique is described in the following section.

5. The extended numerical solution

In order to compute unstable solutions for which the interface $y = \eta(x, t)$ evolves into a configuration possessing overhanging portions, it is necessary to extend the numerical solution technique of Section 4. The mov-

ing coordinate Y and interface location $H(x,t)$ are used, as in Eq. (2.7), and it is still the case that the perturbed velocity potentials $\Phi_1(x,Y,t)$ and $\Phi_2(x,Y,t)$ defined in Eq. (2.8) must have the forms given by expressions (4.1) and (4.2), in order to satisfy Laplace's equation and the appropriate boundary conditions at infinity. It is convenient to define perturbed velocity functions on the moving interface by means of the expressions:

$$\begin{aligned} U_1(x,t) &= (\partial\Phi_1/\partial x)_{Y=H} = -\sum_{n=1}^{N} nP_n(t)\mathrm{e}^{nH(x,t)}\sin(nx),\\ V_1(x,t) &= (\partial\Phi_1/\partial Y)_{Y=H} = \sum_{n=1}^{N} nP_n(t)\mathrm{e}^{nH(x,t)}\cos(nx),\\ U_2(x,t) &= (\partial\Phi_2/\partial x)_{Y=H} = -\sum_{n=1}^{N} nQ_n(t)\mathrm{e}^{-nH(x,t)}\sin(nx),\\ V_2(x,t) &= (\partial\Phi_2/\partial Y)_{Y=H} = -\sum_{n=1}^{N} nQ_n(t)\mathrm{e}^{-nH(x,t)}\cos(nx), \end{aligned} \tag{5.1}$$

and these will be used extensively in the following.

We define an arclength s along the interface (x,H) at any given instant of time by the usual Pythagorean relation

$$\mathrm{d}s^2 = \mathrm{d}x^2 + \mathrm{d}H^2. \tag{5.2}$$

As the wave profile is assumed to be symmetric about the Y-axis, we take $s=0$ at $x=0$ and then write $s=\pm L(t)$ at $x=\pm\pi$. The arclength $L(t)$ along a half wavelength is unknown in advance, and in any event is a function of time t.

It is convenient to define a new arclength variable

$$\xi = \pi s/L(t), \tag{5.3}$$

since the values of this new variable at key points along the wave are known in advance. Specifically, we must have $\xi=0$ at the wave crest $x=0$ and $\xi=\pm\pi$ at $x=\pm\pi$. In terms of this new variable (5.3), the arclength condition (5.2) becomes

$$\left(\frac{\partial x}{\partial \xi}\right)^2 + \left(\frac{\partial H}{\partial \xi}\right)^2 = \frac{L^2(t)}{\pi^2} \tag{5.4}$$

and the interface itself is now sought by means of the Fourier series expansions:

$$\begin{aligned} x(\xi,t) &= \xi + \sum_{n=1}^{N} A_n(t)\sin n\xi,\\ H(\xi,t) &= B_0(t) + \sum_{n=1}^{N} B_n(t)\cos n\xi. \end{aligned} \tag{5.5}$$

Thus the interface (x,H) has a time-dependent parametric representation by means of equations (5.5), and the coefficients $A_n(t)$ and $B_n(t)$ are to be determined.

The chain rule of calculus is now used to transform the kinematic and dynamic boundary conditions along the interface into the new (ξ,t) coordinates. It follows that

$$(\partial H/\partial x)_t = \frac{(\partial H/\partial \xi)_t}{(\partial x/\partial \xi)_t} \tag{5.6}$$

and that

$$(\partial H/\partial t)_x = (\partial H/\partial t)_\xi - \frac{(\partial H/\partial \xi)_t}{(\partial x/\partial \xi)_t}(\partial x/\partial t)_\xi. \tag{5.7}$$

The subscripts in these expressions show the variables that are being held constant in the indicated partial differentiation.

When the expressions (5.6) and (5.7) are used in the first equation in (2.11), the first kinematic condition is obtained in terms of the arclength coordinate ξ in the form

$$\left(\frac{\partial H}{\partial \xi}\right)_t \left(\frac{\partial x}{\partial t}\right)_\xi - \left(\frac{\partial x}{\partial \xi}\right)_t \left(\frac{\partial H}{\partial t}\right)_\xi = \left(\frac{\partial H}{\partial \xi}\right)_t U_1(x,t) - \left(\frac{\partial x}{\partial \xi}\right)_t V_1(x,t). \tag{5.8}$$

The functions $U_1(x(\xi,t),t)$ and V_1 in this kinematic condition (5.8) are as given in Eq. (5.1). The second kinematic condition is obtained by subtracting the two expressions in (2.11) and using the chain-rule results (5.6) and (5.7). This gives the equation

$$[V_2(x,t) - V_1(x,t)](\partial x/\partial \xi)_t = [U_2(x,t) - U_1(x,t)](\partial H/\partial \xi)_t. \tag{5.9}$$

The dynamic condition at the interface is unchanged from Eq. (2.12), although it must be remembered that the time derivatives in that expression assume that x, rather than ξ, is the variable held constant during differentiation of the perturbed velocity potentials in Eqs. (4.1) and (4.2).

The governing equations may now be Fourier decomposed, as in Section 4. The zeroth Fourier mode in the arclength condition (5.4) is obtained by integrating that equation over the interval $\xi \in [-\pi, \pi]$, which corresponds to a complete wavelength. After a little algebra, this yields an explicit expression for the arclength along the surface, as a function of time, in the form

$$L^2(t) = \pi^2 \left[1 + \frac{1}{2}\sum_{n=1}^{N} n^2 (A_n^2(t) + B_n^2(t))\right]. \tag{5.10}$$

Differential equations involving the Fourier coefficients A_n and B_n are now obtained first by differentiating the arclength condition (5.4) to give

$$\frac{\partial x}{\partial \xi}\frac{\partial^2 x}{\partial t \partial \xi} + \frac{\partial H}{\partial \xi}\frac{\partial^2 H}{\partial t \partial \xi} = \frac{L(t)L'(t)}{\pi^2} \tag{5.11}$$

then multiplying this result (5.11) successively by the basis functions $\cos j\xi$ and integrating over a wavelength. This gives the straightforward result

$$\sum_{n=1}^{N} n \mathscr{M}_{jn} A_n'(t) - \sum_{n=1}^{N} n \mathscr{N}_{jn} B_n'(t) = 0 \quad \text{for } j = 1, \ldots, N, \tag{5.12}$$

in which the intermediate quantities:

$$\begin{aligned} \mathscr{M}_{jn}(t) &= \int_{-\pi}^{\pi} (\partial x/\partial \xi)\cos(n\xi)\cos(j\xi)\,\mathrm{d}\xi, \\ \mathscr{N}_{jn}(t) &= \int_{-\pi}^{\pi} (\partial H/\partial \xi)\sin(n\xi)\cos(j\xi)\,\mathrm{d}\xi \end{aligned} \tag{5.13}$$

have been defined for convenience.

Fourier analysis is likewise applied to the first kinematic interface condition (5.8). The zeroth Fourier mode is obtained by integrating over a wavelength, and making use of the result

$$\int_{-\pi}^{\pi} (\partial H/\partial \xi) U_1(x,t)\,\mathrm{d}\xi = \int_{-\pi}^{\pi} (\partial x/\partial \xi) V_1(x,t)\,\mathrm{d}\xi,$$

which may be shown using Eq. (5.1) and integration by parts. The zeroth mode then gives

$$2B_0'(t) = -\sum_{n=1}^{N} n[A_n'(t)B_n(t) + A_n(t)B_n'(t)],$$

which may be integrated at once to yield the expression

$$B_0(t) = -\frac{1}{2}\sum_{n=1}^{N} nA_n(t)B_n(t). \tag{5.14}$$

This result (5.14) is also able to be derived independently from the theorem in Section 4, which may be written

$$\int_{-\pi}^{\pi} H(\xi,t)(\partial x/\partial\xi)\,\mathrm{d}\xi = 0$$

assuming that the mean surface height was initially zero. Making use of the series expressions (5.5) in this equation and evaluating the resulting integrals then gives (5.14) directly.

The remaining Fourier modes in the first kinematic condition are obtained by multiplying Eq. (5.8) by the basis functions $\cos(j\xi)$ and integrating over a wavelength. The coefficient $B_0(t)$ is eliminated from the equation using (5.14), and after a little algebra, the Fourier decomposed form of the first kinematic condition becomes

$$\sum_{n=1}^{N}\left[\frac{1}{2}\pi jnA_j(t)B_n(t) + \mathscr{N}_{jn}\right]A_n'(t) + \sum_{n=1}^{N}\left[\frac{1}{2}\pi jnA_j(t)A_n(t) - \mathscr{M}_{jn}\right]B_n'(t) = -j\sum_{n=1}^{N} S_{jn}^{(1)}P_n(t) \quad \text{for } j = 1,\ldots,N. \tag{5.15}$$

For later convenience, we define (modified) intermediate quantities:

$$\begin{aligned} S_{jn}^{(1)}(t) &= \int_{-\pi}^{\pi} \mathrm{e}^{nH}\sin(nx)\sin(j\xi)\,\mathrm{d}\xi, \\ S_{jn}^{(2)}(t) &= \int_{-\pi}^{\pi} \mathrm{e}^{-nH}\sin(nx)\sin(j\xi)\,\mathrm{d}\xi, \end{aligned} \tag{5.16}$$

the first of which already appears in Eqs. (5.15).

The second kinematic condition (5.9) is now subjected to Fourier analysis, as before. The zero mode is obtained by integrating with respect to the arclength variable ξ, over a complete wavelength. It may then be shown, using integration by parts and the series expressions (5.1), that the two sides of the equation cancel, so that the zeroth Fourier mode of Eq. (5.9) is satisfied as an identity. The remaining modes are obtained by multiplying the equation by the basis functions $\cos(j\xi)$ and integrating over a wavelength in the arclength variable. After some algebra, and again using integration by parts with the definitions (5.1), it follows that the Fourier decomposition of the second kinematic condition gives the remarkably simple result

$$\sum_{n=1}^{N}[S_{jn}^{(1)}P_n(t) + S_{jn}^{(2)}Q_n(t)] = 0 \quad \text{for } j = 1,\ldots,N \tag{5.17}$$

in which the two intermediate quantities are as defined in Eq. (5.16).

In spite of the simplicity of the form (5.17), the aim here is nevertheless to convert this problem from a system of differential-algebraic equations to a straightforward system of ordinary differential equations for the Fourier coefficients, since numerical solution is then more easily done. To accomplish this, Eq. (5.17) are differentiated with respect to time. This involves the use of the series for x and H in Eq. (5.5), and elimination of the coefficient B_0 using (5.14). A little algebra yields the system

$$-\sum_{n=1}^{N}[K_{jn}A_n'(t) + L_{jn}B_n'(t)] + \sum_{n=1}^{N}[S_{jn}^{(1)}P_n'(t) + S_{jn}^{(2)}Q_n'(t)] = 0 \quad \text{for } j = 1,\ldots,N. \tag{5.18}$$

The intermediate quantities $S_{jn}^{(1)}$ and $S_{jn}^{(2)}$ have been defined in (5.16), and we have also introduced the terms:

$$\begin{aligned} K_{jn}(t) &= \int_{-\pi}^{\pi}\left[\frac{1}{2}nB_n(t)(U_2(x,t) - U_1(x,t)) + (V_2(x,t) - V_1(x,t))\sin(n\xi)\right]\sin(j\xi)\,\mathrm{d}\xi, \\ L_{jn}(t) &= \int_{-\pi}^{\pi}\left[\frac{1}{2}nA_n(t) - \cos(n\xi)\right][U_2(x,t) - U_1(x,t)]\sin(j\xi)\,\mathrm{d}\xi \end{aligned} \tag{5.19}$$

for convenience of notation.

Finally, the dynamic interfacial condition (2.12) must also be Fourier analyzed. The zeroth-order mode gives the single equation

$$2\pi D Q_0'(t) + D\sum_{n=1}^{N} C_{0n}^{(2)} Q_n'(t) - \sum_{n=1}^{N} C_{0n}^{(1)} P_n'(t) = -\frac{1}{2} D J_0^{(2)} + \frac{1}{2} J_0^{(1)} - \frac{2\pi(D-1)}{F^2} B_0(t), \tag{5.20}$$

similar to (4.11), and the remaining Fourier modes yield

$$D\sum_{n=1}^{N} C_{jn}^{(2)} Q_n'(t) - \sum_{n=1}^{N} C_{jn}^{(1)} P_n'(t) = -\frac{1}{2} D J_j^{(2)} + \frac{1}{2} J_j^{(1)} - \frac{\pi(D-1)}{F^2} B_j(t) \quad \text{for } j = 1, \ldots, N. \tag{5.21}$$

The intermediate quantities appearing in these expressions are defined to be:

$$\begin{aligned} C_{jn}^{(1)}(t) &= \int_{-\pi}^{\pi} \mathrm{e}^{nH} \cos(nx)\cos(j\xi)\,\mathrm{d}\xi, \\ C_{jn}^{(2)}(t) &= \int_{-\pi}^{\pi} \mathrm{e}^{-nH} \cos(nx)\cos(j\xi)\,\mathrm{d}\xi, \\ J_j^{(1)}(t) &= \int_{-\pi}^{\pi} [U_1^2(x,t) + V_1^2(x,t)]\cos(j\xi)\,\mathrm{d}\xi, \\ J_j^{(2)}(t) &= \int_{-\pi}^{\pi} [U_2^2(x,t) + V_2^2(x,t)]\cos(j\xi)\,\mathrm{d}\xi. \end{aligned} \tag{5.22}$$

The system (5.12), (5.15), (5.18), (5.20) and (5.21) of $4N+1$ differential equations may now be integrated in a reasonably straightforward manner, as in Section 4. We have done this using the standard fourth-order Runge–Kutta method (Atkinson [17], p. 371), although a matrix equation must be solved for the Fourier coefficients at each time step in the method. Nevertheless, this yields results of very high accuracy. As a check, Runge–Kutta–Fehlberg and stiff integration schemes from the computer package *MATLAB* have also been used to follow the evolution of the interface by solving this system of differential equations, and the results are in complete agreement. The integrals that appear in the definitions (5.13), (5.16), (5.19) and (5.22) of the various intermediate quantities are again evaluated using the composite trapezoidal rule, which is arbitrarily accurate for these periodic integrands. Once the solution has been determined at any given value of time t, the surface arclength $L(t)$ can be determined from Eq. (5.10).

6. Presentation of results

The algorithms outlined in Sections 4 and 5 have been run extensively to study the evolution of the interface between the two different fluids. As a check, situations were investigated in the stable case when the density ratio D was less than 1, and as expected, disturbances on the moving interface died away. When $D > 1$, however, the fluid configuration is unstable, and the heavier upper fluid 2 pushes down through the lighter lower fluid 1.

Numerical experiments have shown that, in the unstable case $D > 1$, disturbances to the moving interface grow rapidly with time, as would be expected physically and on the basis of the linearized solution in Section 3. However, at some finite time the numerical integration scheme is seen to break down, so that the evolution of the interface cannot be followed with any confidence beyond that time. This behaviour of numerical solutions to the Rayleigh–Taylor problem was commented upon by Sharp [5], who observed that the failure of numerical codes in this way was poorly understood. The precise time at which this breakdown occurs is very sensitive to initial conditions, such as (3.2), as is entirely to be expected in a physically unstable phenomenon such as this.

The abrupt failure of Fourier-series solutions at a finite time can, in fact, be anticipated purely from a *linearized* solution to the problem. For an arbitrary periodic initial condition that is analytic, all the Fourier modes are required (rather than simply the monochromatic frequency assumed in Eq. (3.1)). An examination of the full linearized solution then shows that the rapid growth of high-frequency Fourier modes must ulti-

mately destroy the analyticity of the initial condition, giving a divergent Fourier series in finite time. Details of this argument are given by Baker et al. [18].

Moore [19] undertook a detailed asymptotic analysis of the *non-linear* equations of motion for the inviscid Kelvin–Helmholtz instability, and argued that the interface can indeed be expected to become non-analytic in finite time. He derived a transcendental equation for the critical time at which this occurs, and suggested that a curvature singularity would form on the interface at this time. The formula shows that the critical time is very sensitive to the amplitude of the initial (sinusoidal) disturbance to the interface, as expected. Thus, at the critical time, the interface is predicted to develop a corner at some point. Inviscid solutions with an infinitely thin interface must then fail for times greater than the critical time. Krasny [20] introduced a numerical method that essentially diffuses the interface over a finite width, and he showed numerically that, for times greater than the critical time, the interface rolls up and forms spiral billows similar to those actually observed for Kelvin–Helmholtz waves. A recent study by Baker and Pham [21] using 'vortex blob methods' gives strong support to the idea that the finite-time formation of a curvature singularity for inviscid flow is the pre-cursor to the growth of spirals at the interface.

Similar analyses have likewise been undertaken for the Rayleigh–Taylor instability. Baker et al. [18] generalized Moore's asymptotic argument, and likewise deduced that a curvature singularity is formed in finite time at some point on the interface. They derived a simple formula for estimating this critical time in dimensionless coordinates. Although their analysis does not strictly apply to the present problem in which the fluid moves with constant speed rather than constant acceleration, we nevertheless give their formula here, in terms of the present variables. The critical time at which a curvature singularity forms on the interface can be estimated from

$$t_c = \frac{1}{r}\ln\left(\frac{1}{\epsilon}\right), \tag{6.1}$$

in which the parameter r is related to the Atwood number, and is given in Eq. (3.6). It turns out that Eq. (6.1) does give reasonable agreement with the numerical results here, for fluids of similar density, for which $D \approx 1$. Tryggvason [22] and Aref and Tryggvason [23] have shown that spiral roll-up also occurs at the interface for Rayleigh–Taylor instability, for times greater than that at which the curvature singularity occurs. (Recent work by Matsuoka and Nishihara [24] has confirmed that similar behaviour occurs also for the Richtmyer–Meshkov instability.)

In order to study further the breakdown of the solutions near the time at which a singularity forms at the interface, we have added a small surface-tension effect to the interface, following Batchelor ([16], p. 150). The only change needed is to add an extra term $\sigma\kappa$ to the left-hand side of the non-dimensional dynamic condition (2.6) at the interface. Here, the new non-dimensional parameter is $\sigma = 2\pi T/(\rho_1 \lambda V^2)$, in which T represents the surface-tension coefficient. The curvature of the interface is given by the quantity $\kappa = \eta_{xx}/[1+\eta_x^2]^{3/2}$. In the coordinate system (x, Y) that moves with the interface, and using the arclength formulation of Section 5, the final form of the dynamic condition at the interface may be shown to be

$$D\frac{\partial \Phi_2}{\partial t} - \frac{\partial \Phi_1}{\partial t} + \frac{1}{2}D[U_2^2(x,t)+V_2^2(x,t)] - \frac{1}{2}[U_1^2(x,t)+V_1^2(x,t)] + \frac{(D-1)}{F^2}H + \sigma\kappa = 0 \quad \text{on } Y = H(x,t), \tag{6.2}$$

replacing Eq. (2.12), Here, the curvature is now

$$\kappa = \frac{\pi^3}{L^3(t)}\left[\frac{\partial^2 H}{\partial \xi^2}\frac{\partial x}{\partial \xi} - \frac{\partial H}{\partial \xi}\frac{\partial^2 x}{\partial \xi^2}\right] \tag{6.3}$$

and the quantity $L(t)$ in this new dynamic condition is the arclength along a half wavelength, and is calculated from Eq. (5.10). It is again required to perform Fourier analysis of Eq. (6.2), to obtain modified forms of the conditions (5.20) and (5.21). These may be derived after a little algebra, but are not given here, in the interests of brevity.

Fig. 2 shows the evolution of a periodic disturbance to the interface, at twelve evenly spaced intervals 0.5 units of time. A single wavelength is shown in the diagram. The initial fluid perturbation speeds in Eqs. (5.1)

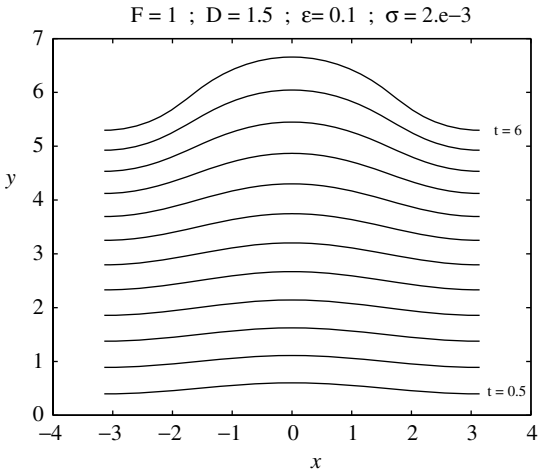

Fig. 2. Evolution of the interface, at equally-spaced times $t = 0.5, 1.0, \ldots, 6.0$. The initial interface was a pure sinusoid, with $B_1(0) = \epsilon = 0.1$. The Froude number is $F = 1$, density ratio is $D = 1.5$ and the surface-tension parameter is $\sigma = 0.002$.

were zero, and the interface was a simple sinusoid of amplitude ϵ, so that $B_1(0) = \epsilon$ and all the other Fourier coefficients were zero at $t = 0$. In this calculation $N = 21$ coefficients were used for each variable, giving a system of 85 differential equations to be solved. The interfacial variables were evaluated at $M = 101$ grid points over the half wavelength $\xi \in [0, \pi]$ and these points were used in the calculation of the appropriate integrals by trapezoidal-rule quadrature. Because this is a full Galerkin scheme, the two integers N and M are completely independent.

The density ratio for the calculation in Fig. 2 was $D = 1.5$ and a small value $\sigma = 0.002$ was taken for the surface-tension parameter. The initial amplitude of the cosine profile for the interface was $\epsilon = 0.1$. As time progresses, the interface grows in amplitude until time $t = 6$, when the numerical algorithm fails suddenly. From a careful inspection of the numerical output, it is evident that the Fourier series suddenly diverge at about $t = 6$.

Fig. 3 gives a more detailed view of the interface at time $t = 6$ for this case. In this picture, the scale on the vertical and horizontal axes is the same, so that the interface is as it would actually appear. The approximate formula (6.1) suggests that a curvature singularity would occur on the interface at about $t_c \approx 5.15$ if the sur-

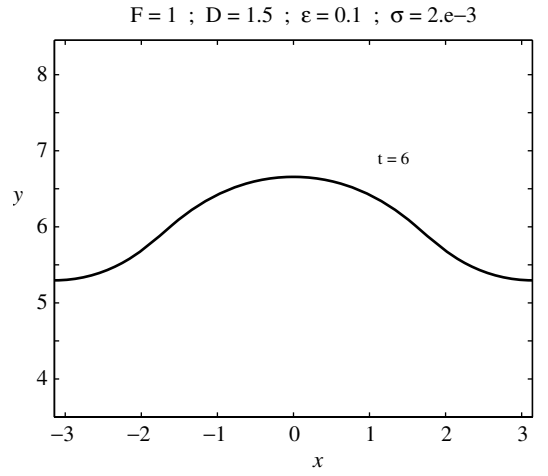

Fig. 3. Interfacial profile at time $t = 6$, for the same case as illustrated in Fig. 2. The scale on each axis is the same.

face tension parameter σ were zero. The presence of a small amount of surface tension evidently allows the solution to continue for a slightly longer time before it too fails.

We have investigated the behaviour of the solution algorithm for a wide variety of parameter values, and in every case it is seen that the numerical solution of the differential equations for the Fourier coefficients fails at some finite time. When $D \approx 1$, that value of time agrees moderately well with the approximate result (6.1), but the agreement is poorer for large density ratio D. Eq. (6.1) suggests that the critical time for singularity formation is very sensitive to the amplitude ϵ of the initial cosinusoidal profile, and this has prompted a further investigation of more general initial conditions. As expected, the growth of the unstable interface is found to be very sensitive to the shape of the initial disturbance.

This sensitivity is illustrated in Fig. 4. Here, the initial conditions were chosen to be $B_1(0) = \epsilon$ and $A_2(0) = 5\epsilon$ with $\epsilon = 0.03$. Thus the periodic perturbations to the interface at time $t = 0$ are not quite sinusoidal, although the differences are only very slight. Nevertheless, the interface now does not evolve as in Fig. 2, but instead ultimately develops over-hanging portions in its profile, as shown in Fig. 4 at time $t = 16$. This is close to the maximum time at which the numerical solution failed. The scale on each axis is the same, so that the profile is as it would actually appear, and the overhanging sections are clearly visible. The approximate formula (6.1) suggests that a curvature singularity does not form until the much later time of about $t_c \approx 22.5$, but this formula cannot be expected to give much guidance in the present situation, since the initial profile used for Fig. 4 is no longer sinusoidal.

The curvature at the interface has been calculated for the solution using Eq. (6.3), and is shown in Fig. 5 for the same parameter values as in Fig. 4. The initial condition was the same, but the result is shown at the slightly earlier time $t = 13$. At that time, there is not yet any evidence of the interface developing overhanging portions, but it is nevertheless clear from Fig. 5 that large curvatures are developing at two points on the interface. This confirms the suggestion that the failure of our numerical solutions at finite time is indeed caused by the formation of curvature singularities, as originally suggested by Moore [19] for the Kelvin–Helmholtz instability. Not surprisingly, numerical errors in the curvature develop rapidly as the solution approaches its final time, and these are evident in Fig. 5 as additional small amplitude oscillations. These are, in part, a result of Gibbs phenomenon, since the Fourier series for curvature is required to represent a discontinuous function; the unstable growth of high-frequency modes then amplifies them in the curvature profile.

Several alternative sets of initial conditions have been studied, including the continuous piecewise-linear profile

$$\eta(x,t) = \begin{cases} \epsilon - (2\epsilon x)/(a\pi(2-a)), & 0 < x < a\pi, \\ -\epsilon a/(2-a), & a\pi < x < \pi \end{cases} \tag{6.4}$$

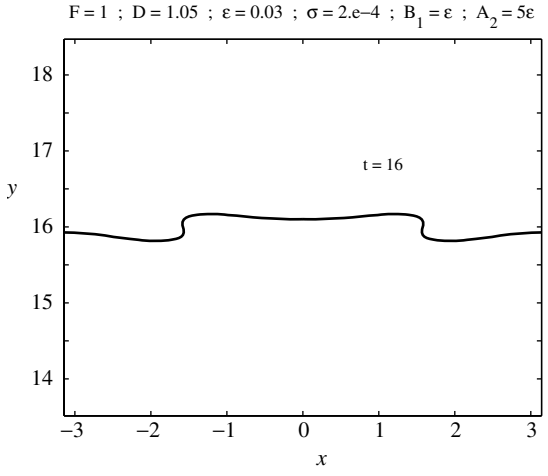

Fig. 4. Interfacial profile at time $t = 16$, computed from the non-sinusoidal initial condition $B_1(0) = \epsilon$, $A_2(0) = 5\epsilon$ and $\epsilon = 0.03$. The Froude number is $F = 1$, density ratio is $D = 1.05$ and the surface-tension parameter is $\sigma = 0.0002$.

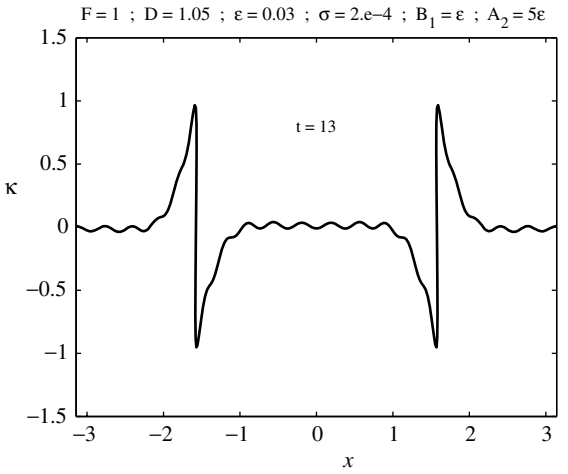

Fig. 5. Interfacial curvature at time $t = 13$, for a solution computed with the same parameters as for Fig. 4.

reflected about the y-axis so as to make it symmetrical. This initial profile thus has the form of a triangular spike of height ϵ, repeated periodically. It follows from Fourier analysis of Eq. (6.4) that the coefficients are:

$$B_0(0) = 0,$$
$$A_j(0) = 0, \quad B_j(0) = \frac{4\epsilon[1-\cos(\pi a j)]}{a\pi^2 j^2(2-a)}, \qquad j = 1, 2, \ldots, N \tag{6.5}$$

at time $t = 0$, in the parametric representation (5.5) of the interface.

These new coefficients (6.5) have been taken as initial conditions for the algorithm in Section 5, and run for an inverted triangular pulse (6.4) with height $\epsilon = -0.1$ and half-width $a = 0.1$ relative to half wavelength. The evolution of the interface is illustrated in Fig. 6 for this case, at twenty times separated by interval 0.4 units of time. The interface begins as an inverted triangular pulse, and grows in amplitude. Here, the density ratio has been chosen to be $D = 1.05$ with Froude number $F = 1$, so that the growth is reasonably slow, as is to be expected from the linear growth rate given in Eq. (3.6). At about time $t = 7$, the interface folds back over itself, thus possessing narrow over-hanging regions in its profile. The numerical algorithm eventually fails at about

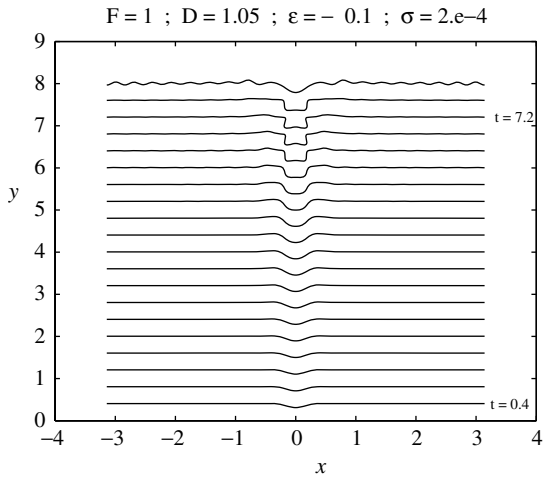

Fig. 6. Evolution of the interface, at equally-spaced times $t = 0.4, 0.8, \ldots, 8.0$. The initial condition was the inverted triangular pulse (6.4) with $a = 0.1$ and $\epsilon = -0.1$. The Froude number is $F = 1$, density ratio is $D = 1.05$ and the surface-tension parameter is $\sigma = 0.0002$.

$t = 8$, when high frequency components in the solution evidently grow rapidly and destroy the convergence of the Fourier series.

A portion of the interface at time $t = 7$ for this case is shown in Fig. 7, with equal scales on both axes. There is clearly a small downward plume of heavier fluid penetrating into lower fluid 1, and the overhanging portions in its interface are evident in the picture.

In an attempt to understand further the folded portions of the interface, illustrated in Fig. 7, we have also sought to incorporate approximately some effects of fluid viscosity near the interface, while still assuming irrotational flow far away. This may be done by retaining some of the terms in the normal component of the dynamic condition at the boundary, given by Batchelor ([16], p. 150). For simplicity, we have assumed that only the lower fluid 1 has viscosity μ_1 and that the upper heavier fluid remains inviscid. Under these assumptions, the simplest form of dynamic boundary condition that approximates the effects of viscosity may be obtained by adding the extra term

$$\frac{2}{Re}\frac{\partial^2 \phi_1}{\partial x^2} \tag{6.6}$$

to the left-hand side of the dimensionless Eq. (2.6). This introduces the extra dimensionless parameter $Re = (\lambda \rho_1 V)/(2\pi\mu_1)$, which is a Reynolds number based on the wavelength λ of the periodic disturbance on the interface. The new equation is then dealt with in a straightforward manner using Fourier analysis as before.

Results are shown in Fig. 8, for an initial inverted (periodic) triangular pulse with half-width $a = 0.1$ and height $\epsilon = -0.1$, as in Eq. (6.4). The Froude number is $F = 1$ and the density ratio is $D = 1.05$. The Reynolds number has been chosen to have the value $Re = 5 \times 10^4$ in the pseudo-viscosity term (6.6), since this value allows a folded interface to evolve. Sixteen profiles are shown, at intervals separated by an interval 0.5 units of time. The surface-tension coefficient σ in Eq. (6.2) has been set to zero.

As time progresses, the disturbance to the interface first grows, and then forms a downward plume with over-hanging sections. A small upward dimple appears at the bottom of the plume, and high-frequency components then ultimately are responsible for a rapid growth of unstable disturbances and the failure of the numerical algorithm at about $t = 8$. An enlarged view of the downward plume near the centre of the wave is presented in Fig. 9, at time $t = 6$. The scale on both axes is the same. The diagram shows more clearly the interface folding inward at the top of the plume, in addition to the small upwardly-pointing dimple at its bottom. Some of the small high-frequency components are also visible at the interface, and for later times these grow rapidly and cause the failure of the numerical solution.

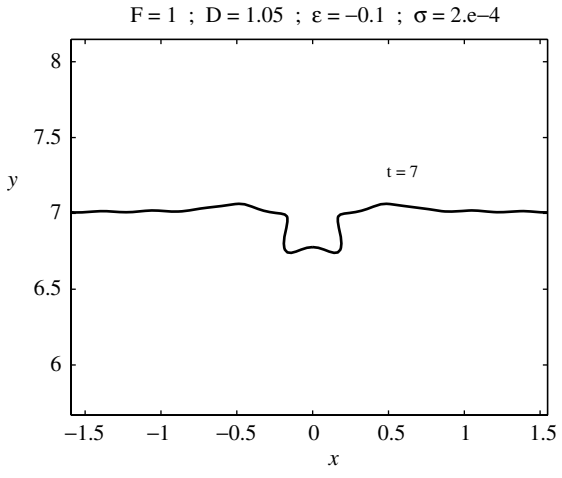

Fig. 7. Interfacial profile at time $t = 7$, for the same case as illustrated in Fig. 6. The scale on each axis is the same.

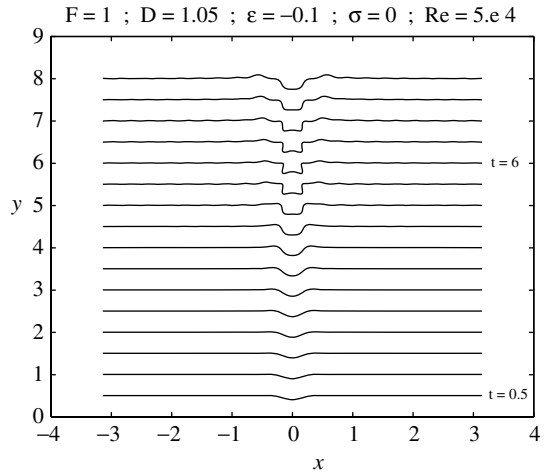

Fig. 8. Evolution of the interface, at equally-spaced times $t = 0.5, 1.0, \ldots, 8.0$. The initial condition was the inverted triangular pulse (6.4) with $a = 0.1$ and $\epsilon = -0.1$. The Froude number is $F = 1$, density ratio is $D = 1.05$ and the Reynolds number is $Re = 50000$.

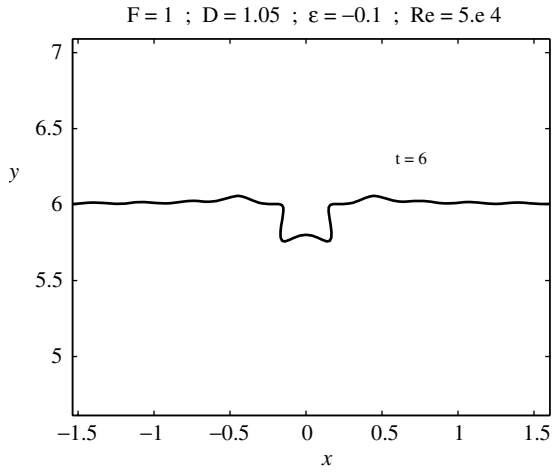

Fig. 9. Interfacial profile at time $t = 6$, for the same case as illustrated in Fig. 8. The scale on each axis is the same.

7. Discussion and conclusion

In this paper, a novel spectral method has been presented for computing the (unsteady) evolution of periodic disturbances at the interface of two fluids. The method uses the Fourier-series representation of the solutions to Laplace's equations in each fluid and assumes a similar series form for the equation of the interface. A system of non-linear ordinary differential equations for the Fourier coefficients is then derived by differentiating one of the kinematic interfacial conditions with respect to time. The resulting set of differential equations is able to be solved using standard integration techniques. In addition, interfaces that fold over and become multiple-valued in position are able to be followed with this technique, by making use of a novel time-dependent arclength formulation.

A type of Rayleigh–Taylor instability has been studied in this paper, using this technique. A lighter fluid is pushing with constant velocity into a heavier fluid, against the acceleration of gravity, and the evolution of small disturbances to the interface has been followed as they grow. Many separate computations have been performed, and in each case it is found that the numerical technique eventually fails. In some sense this is only to be expected, as the flow is unstable, and exponential growth of initial disturbances to the interface is pre-

dicted by the linearized solution in Section 3. The nature of the failure of the non-linear solution, at finite time, is related to the formation of curvature singularities at the interface, as initially suggested by Moore [19] for Kelvin–Helmholtz flow and later by Baker et al. [18] for the Rayleigh–Taylor flow. Singularity formation in the profile curvature is likewise suggested in the present work.

It was found that a slight modification to the initial cosinusoidal profile could generate an interface that evolves folded portions in its profile as time increases. This was made easier to observe by adding a small surface-tension parameter to the dynamic interfacial condition; mathematically, this can be thought of as adding a penalty function to the solution, with surface tension acting as the regularizing parameter. We have also allowed the addition of a type of pseudo-viscosity, so that over-hanging portions may be seen in the evolving interface profile.

The technique presented here is capable of generalization to other situations and geometry. The classical Rayleigh–Taylor problem, with constant acceleration rather than constant velocity, has also been studied with this technique and the results will be presented elsewhere. Similarly, we have applied the method to Kelvin–Helmholtz unstable flow. The method has been found to perform extremely well for *stable* unsteady flows, and gives good results for problems involving withdrawal from a reservoir. Non-planar geometry should also be accessible to a method of this type, and is currently under investigation.

Acknowledgments

This research has been supported in part by Australian Research Council Grant No. DP0450225. Constructive criticism by two Referees is acknowledged.

References

[1] H. Lamb, Hydrodynamics, sixth ed., Dover, New York, 1932.
[2] S. Chandrasekhar, Hydrodynamic and Hydromagnetic Stability, Dover, New York, 1981.
[3] Rayleigh, Investigation of the character of the equilibrium of an incompressible heavy fluid of variable density, Proc. Lond. Math. Soc. 14 (1883) 170–177.
[4] G.I. Taylor, The instability of liquid surfaces when accelerated in a direction perpendicular to their planes. I, Proc. Roy. Soc. Ser. A 201 (1950) 192–196.
[5] D.H. Sharp, An overview of Rayleigh–Taylor instability, Physica 12D (1984) 3–18.
[6] H.J. Kull, Theory of the Rayleigh–Taylor instability, Phys. Lett. 206 (1991) 197–325.
[7] N.A. Inogamov, The role of Rayleigh–Taylor and Richtmyer–Meshkov instabilities in astrophysics: an introduction, Astrophys. Space Phys. 10 (1999) 1–335.
[8] P. Clavin, F. Williams, Asymptotic spike evolution in Rayleigh–Taylor instability, J. Fluid Mech. 525 (2005) 105–113.
[9] M.A. de Avillez, D.L. Berry, Three-dimensional evolution of worms and chimneys in the Galactic disc, Mon. Not. R. Astron. Soc. 328 (2001) 708–718.
[10] N.M. McClure-Griffiths, J.M. Dickey, B.M. Gaensler, A.J. Green, Loops, drips and walls in the Galactic chimney GSH 277+00+36, Astrophys. J. 594 (2003) 833–843.
[11] M. Brouillette, The Richtmyer–Meshkov instability, Annu. Rev. Fluid Mech. 34 (2002) 445–468.
[12] J. Lazier, R. Pickart, P. Rhines, Deep convection, in: G. Seidler, J. Church, J. Gould (Eds.), Ocean Circulation and Climate: Observing and Modelling the Global Ocean, International Geophysics Series, vol. 77, Academic Press, San Diego, 2001, pp. 387–400 (Chapter 5.5).
[13] J.D. Fenton, M.M. Rienecker, A Fourier method for solving nonlinear water-wave problems: application to solitary-wave interactions, J. Fluid Mech. 118 (1982) 411–443.
[14] D.G. Dommermuth, D.K. Yue, A higher-order spectral method for the study of nonlinear gravity waves, J. Fluid Mech. 184 (1987) 267–288.
[15] M.-J. Kim, H.-T. Moon, Y.-B. Lee, S.-K. Choi, Y.-K. Kim, H.-Y. Nam, M. Cho, A spectral method for free surface flows of inviscid fluid, Int. J. Numer. Meth. Fluids 28 (1998) 887–902.
[16] G.K. Batchelor, An Introduction to Fluid Dynamics, Cambridge University Press, Cambridge, 1977.
[17] K.E. Atkinson, An Introduction to Numerical Analysis, Wiley, New York, 1978.
[18] G. Baker, R.E. Caflisch, M. Siegel, Singularity formation during Rayleigh–Taylor instability, J. Fluid Mech. 252 (1993) 51–78.
[19] D.W. Moore, The spontaneous appearance of a singularity in the shape of an evolving vortex sheet, Proc. R. Soc. Lond. A 365 (1979) 105–119.
[20] R. Krasny, Desingularization of periodic vortex sheet roll-up, J. Comput. Phys. 65 (1986) 292–313.
[21] G. Baker, L.D. Pham, A comparison of blob methods for vortex sheet roll-up, J. Fluid Mech. 547 (2006) 297–316.
[22] G. Tryggvason, Numerical simulations of the Rayleigh–Taylor instability, J. Comput. Phys. 75 (1988) 253–281.

[23] H. Aref, G. Tryggvason, Model of Rayleigh–Taylor instability, Phys. Rev. Lett. 62 (1989) 749–752.
[24] C. Matsuoka, K. Nishihara, Vortex core dynamics and singularity formations in incompressible Richtmyer–Meshkov instability, Phys. Rev. E 73 (2006) 026304 1–026304 16.